Earth and Planetary Science Letters 341-344 (2012) 186–194

Contents lists available at SciVerse ScienceDirect

Earth and Planetary Science Letters

journal homepage: www.elsevier.com/locate/epsl

Letters

Chondrule fragments from Comet Wild2: Evidence for high temperature processing in the outer Solar System

J.C. Bridges [a,*], H.G. Changela [b,c], S. Nayakshin [d], N.A. Starkey [e], I.A. Franchi [e]

[a] Space Research Centre, Department of Physics & Astronomy, University of Leicester, Leicester LE1 7RH, UK
[b] George Washington University, Department of Physics, 725 21st Street, NW, Washington, DC 20052, USA
[c] Naval Research Laboratory, 4555 Overlook Ave. SW, Washington, DC 20375, USA
[d] Department of Physics & Astronomy, University of Leicester, Leicester LE1 7RH, UK
[e] Department of Physical Sciences, Planetary & Space Sciences, Open University, Milton Keynes MK7 6AA, UK

ARTICLE INFO

Article history:
Received 29 September 2011
Received in revised form
28 May 2012
Accepted 7 June 2012
Editor: T. Elliot
Available online 11 July 2012

Keywords:
Comet Wild2
Al-rich chondrules
oxygen isotopes
NanoSIMS
carbonaceous chondrites
giant planetary embryos

ABSTRACT

Terminal grains from C2063,1,154,1,0 (Track 154) and C2061,1,113,5 (Track 113) from the *Stardust* collection of Comet Wild2's coma have been studied by TEM and NanoSIMS. Terminal grain 2 of C2063,1,154,1,0 consists of an Al-rich diopside (En 97–99%, Al_2O_3 9–11 wt%), pigeonite (En 85% Wo 15% with TiO_2 and Al_2O_3 contents of 0.5 and 5.2 wt%) and minor forsterite and enstatite. The mineral assemblage and Al-rich, Ti-poor composition of the grain are consistent with being a fragment of an Al-rich chondrule, similar to those present in carbonaceous chondrites. The oxygen isotopic composition of the C2063,1,154,1,0 grain was determined by NanoSIMS analyses and found to be $\delta^{17}O$ -10.6 ± 5.7‰, $\delta^{18}O$ -7.5 ± 2.5‰ and $\delta^{17}O$ $+1.4\pm4.3$‰, $\delta^{18}O$ -6.5 ± 1.6‰ (1σ errors) for the two sections. These figures are distinct from CAIs and consistent with an origin as Al-rich chondrule fragments. Terminal grain 5 of C2061,1,113,5 consists of low Ca pyroxene En 86–87% Fs 10–11% Wo 3–4% and ≤ 2 wt% Al_2O_3 and in one section 5–10% of a Na-rich silicate phase. This assemblage may be a fragment of a low-Ca pyroxene-bearing chondrule and mesostasis. The original chondrule diameter for the C2063,1,154,1,0 and C2061,1,113,5 samples, by analogy with carbonaceous chondrite chondrules, might have been in the range 0.2–1.0 mm. If they were of that size, then the presence of large grains of high temperature material (e.g. ≥ 1500 K for such refractory assemblages) could be explained through commonly invoked models of radial drift from inner to outer Solar System, but only if the chondrules were first fragmented to dust within the inner Solar System. An alternative scenario is that some chondrule formation was associated with high temperature processing and planetesimals in the outer Solar System.

1. Introduction

One of the notable results of recent cometary studies and the *Stardust* mission to return dust samples from the coma of 81P/Comet Wild2 has been the identification of a large proportion of high temperature (i.e. >1000 K) phases. Despite the inevitably fragmented nature of the samples which were collected at a closing velocity of 6 km s^{-1}, remarkable new information about cometary material has been provided which can be the basis for a better understanding of some early Solar System processes. The mass fraction of crystalline silicates from Comet Wild2, and in the ejecta of Comet 9P/Tempel 1, is surprisingly high (Zolensky et al., 2006), perhaps as great as ~0.5–0.65 for the *Stardust* results (Westphal et al., 2009). In addition to this, a Calcium Aluminium Inclusion (CAI) and FeMg chondrule fragments have been identified within the Comet Wild2 samples (Ishii et al., 2008; Butterworth et al., 2010; Nakamura et al., 2008).

Chondrules are approximately mm-sized roughly spherical, silicate melt droplets composed mainly of olivine and low-Ca pyroxene set in a feldspathic or glassy matrix (e.g. see Scott and Krot (2003) for a review of chondrules). They are a major constituent of most chondrite groups (e.g. 15–70% of chondrule-bearing carbonaceous chondrites). The maximum temperatures of crystallisation are taken to be approximately around the liquidus of 1200–1500 K but peak temperatures during melting of precursors may have been higher (Desch et al., 2010). Many CAIs experienced even greater temperatures (Davis and Richter, 2003). Another set of chondrules are refractory, Al-rich, having bulk compositions around 10 wt% Al_2O_3 or greater (Bischoff and Keil, 1983). They are most frequently found in carbonaceous chondrites but also exist in ordinary chondrites. They are intermediate in composition between FeMg chondrules and some CAIs.

* Corresponding author.
E-mail address: j.bridges@le.ac.uk (J.C. Bridges).

0012-821X
http://dx.doi.org/10.1016/j.epsl.2012.06.011

Chondrules and CAIs are particles normally associated with asteroidal planetesimals that are the chondrite meteorite parent bodies. Thus the presence of these particles in a Jupiter Family comet which originated beyond the orbit of Neptune at 30 AU appears anomalous. To account for their presence, turbulent radial drift or X-wind models have been invoked (Simon et al., 2008). These models propose that mm- to cm-sized particles could be transported from the relatively hot, inner portions of the protoplanetary disc out to the comet-forming region (Bockelée-Morvan et al., 2002; Ciesla, 2007; Shu et al., 1997). However, as pointed out recently by Hughes and Armitage (2010), such models which seek to explain outward transport of relatively large particles experience a rapid drop off in transport efficiency with time. High-temperature material would have to be quickly incorporated into icy bodies to avoid fallback to small radii. An alternative scenario involves the formation of early planetesimals within isolated hot, dense regions of the outer Solar System (e.g. Nayakshin et al., 2011).

In this paper we present new mineralogical and oxygen isotopic evidence for the presence of high temperature, chondrule fragments of refractory composition within Comet Wild2. We explore the implications of their presence in a primitive body which originated at ~25–30 AU in the light of models involving the transportation of particles from the inner Solar System or formation in-situ within the outer Solar System.

2. Sample and methods

2.1. Mineralogy

TEM sections from C2063,1,154,1,0 (Track 154) and C2061,1,113,5 (Track 113) were allocated to us by the *Stardust* Allocation Committee as unscreened Type A and B tracks. C2063,1,154,1,0 is a 920 μm length bulbous Type B track, containing 6 grains in terminal positions. It was extracted from tile C2063, by NASA-Johnson Space Center (Nakamura-Messenger et al., 2011), followed by dissection of Terminal Particle 2 and preparation of a potted butt. The '154' in the identifier refers to the track number throughout all of the identified cometary tracks. Following microtome preparation by NASA-JSC, three separate grids with two 70–90 nm thick sections on each grid were provided for this study: C2063,1,154,1,14, C2063-1-154,1,15 and C2063,1,154,1,17. C2061,1,113,5 is a 1.5 mm length Type B track with 8 distinct terminal particles. Four 70–90 nm thick sections prepared by microtome at NASA-JSC from terminal grain 5, C2061,1,113,5,1-4, were studied with TEM at Leicester. Track type classification after Burchell et al. (2008).

TEM was performed with the University of Leicester, Advanced Microscopy Centre, Jeol 2100 fitted with a LaB_6 source. The samples were analysed at 200 kV and 106–111 μA emission currents. Analyses included Bright Field (BF) and Dark Field (DF) imaging, Selected Aperture Electron Diffraction (SAED), High Resolution TEM and Scanning TEM (STEM) BF and DF. C2063,1,154,1,0 samples were also imaged with an FEI *Sirion* FEG-SEM at 4 kV.

Energy dispersive X-ray (EDX) analyses were made with a PGT *Gamma Tech* system and performed using Cliff Lorimer *K*-factors (Cliff and Lorimer, 1975). *K* factors for Mg, Ca and Fe were calculated using Focused Ion Beam (FIB) preparation of mineral standard wafers: Barwell L6 olivine (Mg#=0.75) and diopside, San Carlos olivine (Mg#=0.91), kyanite (Al_2SiO_5). *K*-factors for Mg, Fe, Ca and Al (normalised to Si) were found to be 1.25, 1.36, 1.1 and 1.0. *K* factors for other elements were used from the default values within the TEM EDX *Spirit* software. The *K* factor calibrations were checked with Barwell pyroxenes analysed by wavelength dispersive spectroscopy (Changela, 2011). Representative errors for elemental atomic concentrations are Si 4.4%, Mg 5.8%, Fe 5.1% and Ca 2.2%. Typically, 25 nm spot sizes and 600 s acquisition times were used for EDX analyses. The beam sensitive and relatively labile nature of the Na-rich phase in the C2061,1,113,5 sample mean that only qualitative analyses are reported for it.

2.2. Oxygen isotopes

Oxygen isotope measurements of the Stardust sections C2063,1,154,1,15 and C2063,1,154,1,17 were performed with the NanoSIMS 50L at the Open University. NanoSIMS 50L isotope imaging mode allows for the limited material available in the thin microtome sections to be maximised for isotopic analysis.

After all other analyses (e.g. SEM, TEM) on the sections were complete, the back of the TEM grids containing the microtomed sections were reinforced with a 200 nm gold coat and a further 20 nm gold coat was deposited on the top of the sections to facilitate charge dissipation. The sections were mounted in a Cameca NanoSIMS TEM grid holder. A 2 pA Cs^+ probe was rastered over a $10\times10\ \mu m^2$ area for pre-sputter and an $8\times8\ \mu m^2$ area for analysis of both *Stardust* sections and olivine standards. The mass resolution was set to over 10,000 which allows for ^{17}O to be resolved from ^{16}OH. Measured ^{16}OH was a factor of 10 higher than the ^{17}O peak for the particles in the *cometary* sections and around a factor of 20 higher than the ^{17}O peak for the aerogel. Negative secondary ions of ^{16}O, ^{17}O, ^{18}O, ^{28}Si, $^{24}Mg^{16}O$ and $^{56}Fe^{16}O$ were measured on electron multiplier detectors. Charge compensation (electron gun) was used throughout measurements on both standards and *Stardust* sections. Reproducibility tests and calibration measurements were performed on flat, polished San Carlos olivine. $\delta^{17}O$ and $\delta^{18}O$ were normalised to standard mean ocean water (SMOW) from San Carlos olivine measurements that bracketed the analysis. Image analyses on the standards lasted for 30 min and on *Stardust* sections for 1 h. Total counts of ^{16}O were $\approx4.5\times10^8$ on San Carlos olivine images and $\approx1.7\times10^8$ on the cometary sections. In both cases the ^{16}O peak was measured every 10 min during analyses in order to determine peak drift and corrections were applied accordingly to the peak positions of the other species. The reproducibility obtained from comparable areas to those of the grains in the Stardust sections in a set of five images on San Carlos olivine was 0.9‰ for $\delta^{18}O$, 4.2‰ for $\delta^{17}O$ and 4.3‰ for $\Delta^{17}O$ (1σ). Similar analyses on flat, polished Eagle Station olivine calibrated

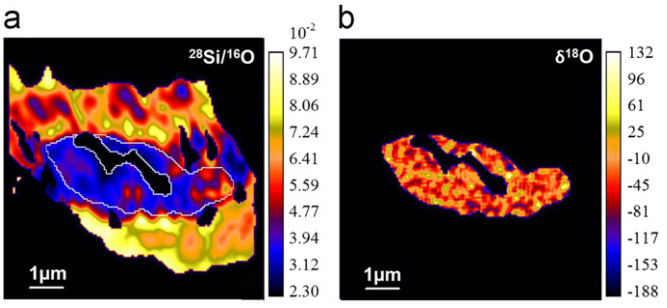

Fig. 1. NanoSIMS measurements processed with L'image software. (a) Example of contrast in $^{28}Si/^{16}O$ that was used to define ROI for particle C2063,1,154,1,15, along with other elements and TEM images, (b) particle ROI. The ROI does not match exactly the shape of the particle apparent in TEM images (see Fig. 2) which may be partly the result of small movement of some particle fragments between TEM and NanoSIMS analyses. A conservative estimate of the grain outline was used in order to minimise the risk of contamination by aerogel in the particle ROI. The isotopic variation within the particle is largely isotropic, the observed variation is mainly the result of statistical noise, primarily from pixels with low ^{16}O counts. Raster size is 8×8 μm in all cases.

against San Carlos olivine gave correct values within error of the true value as measured by laser fluorination.

Results were processed using L'image software and corrected for position drift and quasi-simultaneous arrival (QSA) effect. The difference in matrix effect between the low-FeO pyroxene and the olivine standard is thought to be negligible compared to the precision and a correction is not applied, in line with other SIMS studies (Ito et al., 2004; Kita et al., 2010; McKeegan et al., 1998; Russell et al., 2000). The aerogel surrounding the particle was discriminated from the particle on the basis of combined $^{28}Si/^{16}O$ and ^{16}O counts in the L'image software, guided by the approximate particle outline revealed in TEM images (Fig. 1).

3. Mineralogy

C2063,1,154,1,0: The grain slices on the TEM grids range up to 6.5 by 2.4 μm (Fig. 2) and in total ~20 μm^2 of this terminal particle has been analysed. The sample is mostly (97%) composed of Al-rich, Ti-poor diopside of average composition $En_{50}Wo_{50}$, Mg# of 0.9–1.0 and wt% Al_2O_3 with TiO_2 contents 0–1.8 wt% (analyses in Table 1). A representative Al-rich diopside spectrum is shown in Fig. 3. Minor amounts of enstatite and forsterite, Mg# 0.99–1.00, Al_2O_3 ≤1.9 wt% and pigeonite are also present. The pigeonite composition is $En_{83-87}Wo_{13-17}$ with TiO_2 and Al_2O_3 contents of 0.2–0.6 and 4.4–7.8 wt% respectively. Minor amounts of Fe–Ni and Fe sulphide have been identified at the margins of the grain.

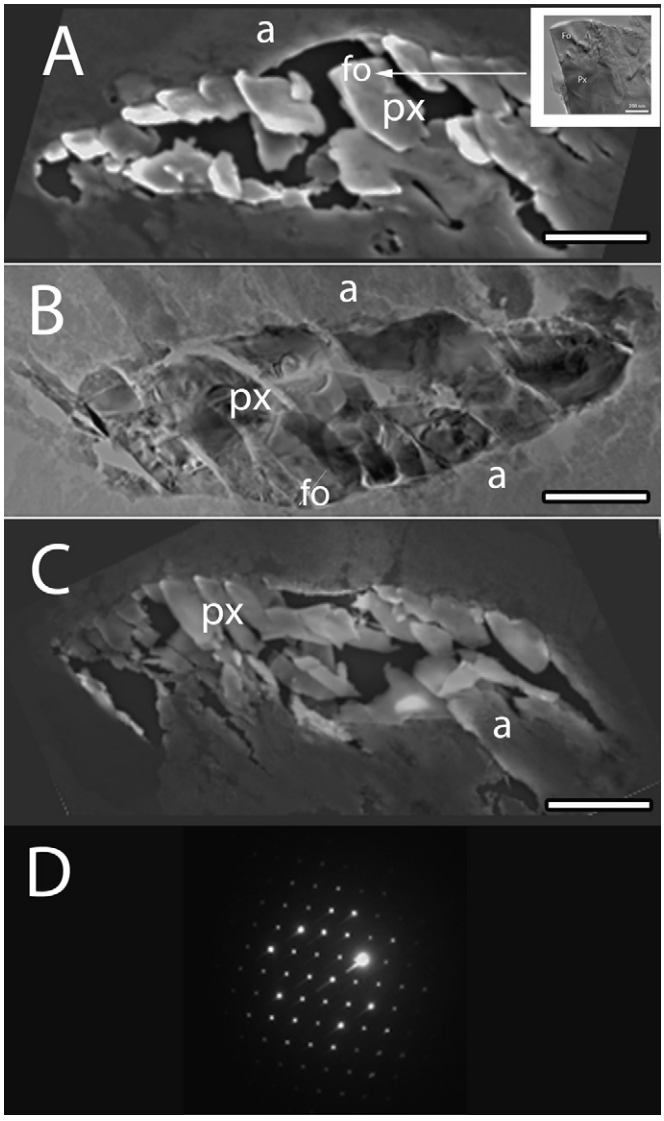

Fig. 2. C2063,1,154,1,0 terminal grain 2 images. (A) Section C2063,1,154,1,14 FEG-SEM. Inset shows BF image of forsterite grain, scale bar 200 nm. (B) Section C2063-1-154-1-15 TEM Bright Field image. (C) Section C2063,1,154,1,17 FEG-SEM. (D) Selected aperture electron diffraction of diopside in C2063,1,154,1,14, [0–10] zone axis. The shards and partially fragmented nature of the sections is the result of fracturing during microtome preparation. a: aerogel, px: Al-rich clinopyroxenes and enstatite. Arrow indicates position of forsterite in C2063,1,154,1,17. 1 μm scale bars.

The pyroxene compositions are plotted in Fig. 4 together with the overlapping fields for Al-rich diopside (+pigeonite) chondrules from HH237, QUE9411/94627, which are carbonaceous chondrites with CH, CR affinities (Krot et al., 2001). In Fig. 5 the TiO_2 vs. Al_2O_3 contents of the pyroxenes are shown. The Al-diopside in the C2063,1,154,1,0 sample also has a similar composition for these compounds to that from Al-diopside rich chondrules identified in HH237 and QUE94411/94627 (Krot et al., 2001). In Fig. 6, both the Al-diopside-rich chondrules from carbonaceous chondrites described by Krot et al. (2001) and the C2063,1,154,1,0 analyses lie within the Fo+L field. The pyroxene in the particle has a lower range of TiO_2 contents than that associated with high Ca, Al pyroxene from CAIs. No Cr_2O_3 or CaO was detected in the pyroxene.

C2061,1,113,5: 15 μm^2 of this terminal grain 5 particle were studied and it was found to consist of 90–95% low-Ca pyroxene and 5–10% of a Na-rich glassy phase (Fig. 7). The pyroxene is En 86–87% Fs 10–11% Wo 3–4% and ≤2 wt% Al_2O_3 (Fig. 4, Table 1). The EDX spectrum of the Na-rich phase is shown in Fig. 3. It is qualitatively consistent with a Na-, Al-rich, silica undersaturated, nepheline-like composition. No Na-alkali enrichment was detected in the pyroxene and no other phases were identified. In a study of 3 of the other terminal particles from this track, Nakamura-Messenger et al. (2011) also identified nepheline ($NaAlSiO_4$) within orthoenstatite with minor clinoenstatite. In addition, these other terminal particles contained minor forsterite and (Al-poor) diopside.

4. Oxygen isotopes

The oxygen isotopic composition, with 2σ errors, of the particle in section C2063,1,154,1,15 is $\delta^{17}O = -10.6 \pm 11.4‰$ and $\delta^{18}O = -7.5 \pm 5.0‰$ and section C2063,1,154,1,17 of the particle is $\delta^{17}O = 1.4 \pm 8.6‰$ and $\delta^{18}O = -6.5 \pm 3.2‰$. These compositions are plotted in Fig. 8A and B (analyses in Table 2). The corresponding $\Delta^{17}O$ values are −6.7‰ and 4.8‰. The composition is distinct from that of CAIs, including the *Inti* CAI identified in Comet Wild 2 (Simon et al., 2008) which has a composition around $\delta^{17}O$ −40‰, $\delta^{18}O$ −40‰, including Al-rich diopside, although the analysis spots for *Inti* cross cut different mineral phases (McKeegan et al., 2006). The only CAI pyroxene field it does overlap within error is that of the ^{16}O-poor end of the diopside field for Type C CAIs (Krot et al., 2008). It does overlap within 2σ errors, the fields for bulk chondrules from carbonaceous chondrites, the fields for Al-diopside-rich bulk chondrules in CB chondrites and QUE 94627 (Krot et al., 2001, 2006), Al-rich chondrules in ordinary chondrites and CR chondrites and Al-rich pyroxene from chondrules in ordinary chondrites. In general bulk Al-rich chondrules have a more ^{16}O-rich oxygen isotopic composition than FeMg chondrules e.g. compare the field for Al-rich chondrules from CR chondrites to that of FeMg chondrules from carbonaceous chondrites in Fig. 8B. Similarly, Al-rich chondrules from ordinary chondrites are ^{16}O-rich compared to FeMg chondrules (e.g. Li et al., 1998; Russell et al., 2000). This has been interpreted as formation from more ^{16}O-rich solids than were the

Table 1
TEM-EDX mineral data.

	Track#154																		Track#113		Track#154
wt%	Di	Di	Di	Di	Di	Di	Di	Di	Di	Di	Di	Di	Di	Di	Pig	Pig	Pig	En	En	En	En	Fo
MgO	13.5	16.4	19.8	16.6	12.7	13.6	14.5	14.7	13.1	12.4	14.3	13.4	17.2	14.7	33.5	36.4	31.6	35.8	37.0	32.8	29.0	55.5
CaO	20.9	23.2	23.0	23.7	21.0	21.0	21.9	21.3	18.3	17.5	20.7	20.8	23.5	21.1	6.8	4.0	7.6	0.2	0.0	1.4	2.2	0.0
TiO_2	0.9	0.6	0.4	1.1	1.1	1.2	0.4	0.4	1.0	1.3	1.2	1.3	0.0	1.1	0.4	0.6	0.2	0.5	0.3	0.0	0.0	0.0
FeO	0.0	0.0	0.0	0.4	0.5	0.4	0.0	0.0	0.5	0.5	0.5	0.5	0.0	0.4	0.4	0.4	0.3	1.3	0.8	7.0	7.8	0.0
Cr_2O_3	0.0	0.0	0.0	0.0	0.0	0.0	0.0	0.0	0.0	0.0	0.0	0.0	0.0	0.0	0.0	0.0	0.0	0.0	0.0	1.0	1.4	0.0
CoO	0.0	0.0	0.0	0.3	0.4	0.3	0.0	0.0	0.4	0.4	0.4	0.4	0.0	0.3	0.0	0.0	0.0	0.0	0.0	0.0	0.0	0.0
Al_2O_3	11.4	10.8	8.8	9.9	9.7	10.2	10.8	11.0	9.9	12.2	10.9	10.8	10.4	10.6	6.3	4.4	7.8	1.9	1.3	0.0	0.0	0.5
SiO_2	53.3	48.9	48.0	48.2	54.5	53.1	52.5	52.6	56.9	55.5	52.1	52.9	48.9	51.8	52.6	54.3	52.4	60.4	60.7	57.9	59.7	44.1
Atom																						
Si	1.9	1.8	1.8	1.7	2.0	1.9	1.9	1.9	2.0	2.0	1.9	1.9	1.8	1.8	1.8	1.8	1.8	2.0	2.0	2.0	2.1	1.0
Al	0.1	0.2	0.2	0.3	0.0	0.1	0.1	0.1	0.0	0.0	0.1	0.1	0.2	0.2	0.2	0.2	0.2	0.0	0.0	0.0	0.0	0.0
Sum	2.0	2.0	2.0	2.0	2.0	2.0	2.0	2.0	2.0	2.0	2.0	2.0	2.0	2.0	2.0	2.0	2.0	2.0	2.0	2.0	2.1	1.0
Mg	0.7	0.9	0.9	0.9	0.7	0.7	0.8	0.8	0.7	0.7	0.8	0.7	0.9	0.8	1.7	1.8	1.6	1.8	1.9	1.7	1.5	1.9
Ca	0.8	0.9	0.9	0.9	0.8	0.8	0.8	0.8	0.7	0.7	0.8	0.8	0.9	0.8	0.3	0.1	0.3	0.0	0.0	0.1	0.1	0.0
Ti	0.0	0.0	0.0	0.0	0.0	0.0	0.0	0.0	0.0	0.0	0.0	0.0	0.0	0.0	0.0	0.0	0.0	0.0	0.0	0.0	0.0	0.0
Al	0.4	0.2	0.2	0.2	0.4	0.3	0.3	0.3	0.4	0.5	0.3	0.4	0.2	0.3	0.1	0.0	0.1	0.1	0.1	0.0	0.0	0.0
Fe	0.0	0.0	0.0	0.0	0.0	0.0	0.0	0.0	0.0	0.0	0.0	0.0	0.0	0.0	0.0	0.0	0.0	0.0	0.0	0.2	0.2	0.0
Cr	0.0	0.0	0.0	0.0	0.0	0.0	0.0	0.0	0.0	0.0	0.0	0.0	0.0	0.0	0.0	0.0	0.0	0.0	0.0	0.0	0.0	0.0
Co	0.0	0.0	0.0	0.0	0.0	0.0	0.0	0.0	0.0	0.0	0.0	0.0	0.0	0.0	0.0	0.0	0.0	0.0	0.0	0.0	0.0	0.0
Sum	1.9	2.0	2.0	2.0	1.9	1.9	1.9	1.9	1.9	1.9	2.0	2.0	2.0	1.9	2.0	2.0	2.0	2.0	2.0	2.0	1.9	1.9
O	6.1	6.0	6.0	6.0	6.1	6.1	6.1	6.1	6.1	6.1	6.1	6.1	6.0	6.0	6.0	6.0	6.0	6.0	6.0	6.0	6.1	4.0
%Wo	52.7	50.4	50.4	50.4	53.8	52.1	52.2	51.0	49.7	49.7	50.5	52.3	49.5	50.8	12.7	7.2	14.7	0.3	0.0	0.1	0.1	
%En	47.3	49.6	49.6	49.0	45.3	47.0	47.8	49.0	49.2	49.1	48.6	46.7	50.5	49.2	86.7	92.2	84.8	97.8	98.8	0.8	0.8	
%Fs	0.00	0.00	0.00	0.60	0.93	0.83	0.00	0.00	1.06	1.18	0.88	0.91	0.00	0.00	0.61	0.55	0.47	1.91	1.17	0.11	0.13	
Mg#	1.00	1.00	1.00	0.99	0.98	0.98	1.00	1.00	0.98	0.98	0.98	0.98	1.00	1.00	0.99	0.99	0.99	0.96	0.97	0.88	0.87	1.0

Di: diopside, Pig: pigeonite, En: enstatite, Fo: forsterite. See methods section for Cliff Lorimer *K* factors used in this study.

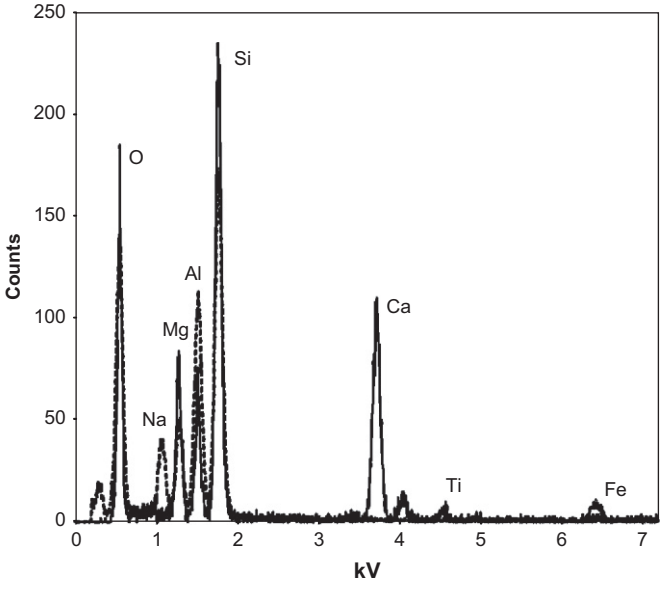

Fig. 3. TEM-EDX representative spectra of Al-diopside (black line) from C2063,1,154,1,0 terminal grain 2 and Na-rich glass from C2061,1,113,5 terminal grain 5 (dashed line). Labelled peaks are Kα lines.

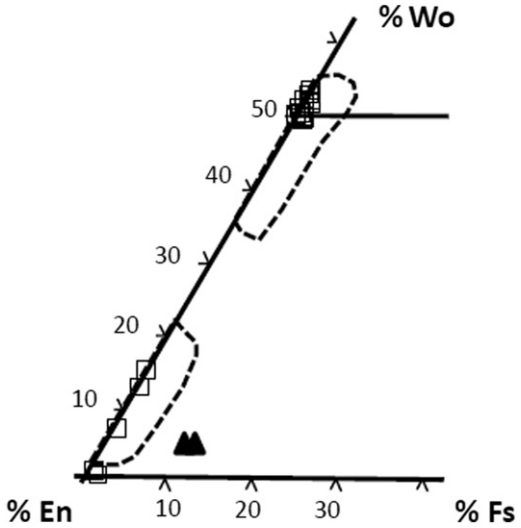

Fig. 4. Part of the pyroxene quadrilateral, % wollastonite (Wo), enstatite (En), ferrrosilite (Fs). Diopside, pigeonite and enstatite TEM-EDX analyses ($N=19$) from C2063,1,154,1,0 terminal grain 2 and (triangles) low-Ca pyroxene from C2061,1,113,5, terminal grain 5. Also shown in dashed line fields are the pyroxene compositions for Al-rich diopside (+pigeonite) chondrules from HH237, QUE9411/94627, which are carbonaceous chondrites with CH, CR affinities (Krot et al., 2001). C2063,1,154,1,0 and 1C2061,1,113,5 analyses are given in Table 1.

precursors for FeMg chondrules (Krot et al., 2001). However, individual minerals within FeMg chondrules can also have ^{16}O-rich compositions (e.g. Jones et al., 2004). Such scatters of chondrule isotopic compositions with chondrite groups may be the result of diffusion and mineral-specific exchange with ^{16}O-poor gases through existing solid chondrules (Bridges et al., 1999), or through chondrules as they were crystallising (Jones et al., 2004).

Two NanoSIMS oxygen isotope analyses of terminal particles 2,3 from Track C2061,1,113,5 (Nakamura-Messenger et al., 2011) similar to the terminal particle 5 studied here are also plotted in Fig. 8B.

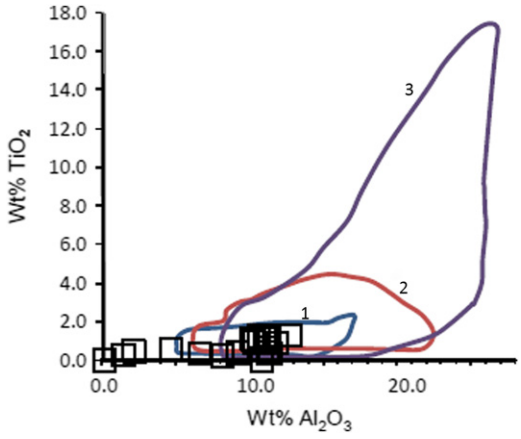

Fig. 5. TiO_2 vs. Al_2O_3 composition of pyroxene (squares $N=19$) in terminal particle #2 of Track #154. The Al-diopside has a similar composition to that from Field 1. Al-diopside rich chondrules identified in HH237 and QUE94411/94627—meteorites which have affinities to CH and CR chondrites. The particle's pyroxene has a lower range of TiO_2 contents than that associated with high Ca pyroxene from typical 2. pyroxene-spinel inclusions and 3. pyroxene from hibonite-rich CAIs. Pyroxene data fields are from Krot et al. (2001).

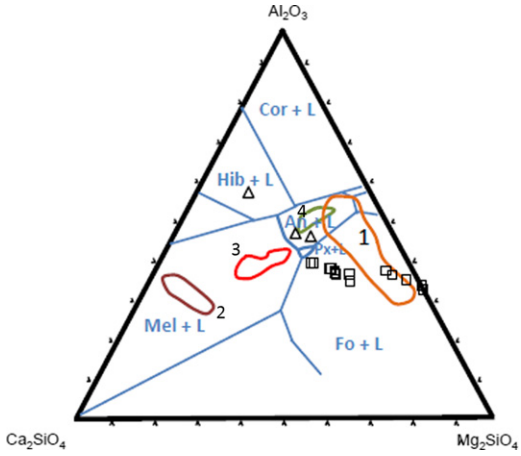

Fig. 6. Pyroxene TEM-EDX analyses ($N=19$) from terminal particle 2 of Track #154. Bulk compositions of 1. Al-rich chondrules and 2. Type A (melilite-rich), 3. Type B (Al, Ti-pyroxene-rich) and 4. Type C (plagioclase–pyroxene rich) CAIs from MacPherson (2003). Open triangle—pyroxene from the *Inti* CAI (Ishii et al., 2008; Chi et al., 2009). The Track #154 pyroxene analyses lie within the Fo+L field and overlap with the bulk Al-rich chondrules' analyses, but are distinct from the CAI bulk compositions and most pyroxene from the *Inti* CAI. Plot is a CMAS-type projection from spinel (Cox et al., 1979).

5. Discussion

5.1. Chondrite, IDP or CAI affinities?

Al-diopside chondrules in CH chondrites and the metal-rich chondrites QUE 94627, QUE 94411 and HH 237 contain Al-diopside with low Ti and Cr contents, inclusions of forsterite, Al-rich Ca-poor pyroxene and anorthitic mesostasis with occasional spinel (Krot et al., 2001). Compositionally the Al-diopside and pigeonite is similar to that from the C2063,1,154,1,0 grain studied here. The presence of minor forsterite is consistent with such an identity. However, if the C2063,1,154,1,0 particle is a fragment of such a chondrule, the mesostasis or spinel part has either not been identified or not been preserved. It is clear that the C2063,1,154,1,0 grain does not have CAI affinities, in particular the low Ti contents make such a link unlikely. The major element compositional features of this C2063,1,154,1,0 particle (e.g. Fig. 4–6) are much more similar to Al diopside chondrules than CAIs. In contrast the *Inti* particle from Comet Wild 2 contains pyroxene of similar composition to CAIs from carbonaceous chondrites (Simon et al., 2008).

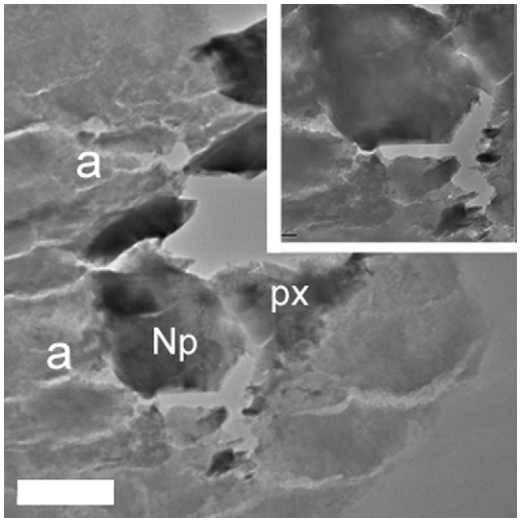

Fig. 7. Track 113 TEM Bright Field images, section C2061,1,113,5,4 with inset showing higher magnification view around Na-rich phase. Px: enstatite, Np: Na–Al-silicate nepheline-like phase, a compressed aerogel from collector tile. Scale bar is 1 μm.

Anhydrous chondritic, porous interplanetary dust particles (IDPs) are generally assumed to be of cometary origin (e.g. Rietmeijer, 1998). There are reports of IDPs containing Al-diopside and Ca–Ti–Al-rich clinopyroxene. Tomeoka and Buseck (1985) described an IDP with carbonaceous chondrite affinities called *Skywalker* that contained refractory pyroxene associated with phyllosilicate. This hydrated IDP contained a diopside grain with a TiO_2 content of 0.6 wt% and Al_2O_3 of 14.5 wt%. The Zolensky and Barrett (1994) study of a suite of chondritic IDPs identified diopside in 40% of hydrous IDPs. However, studies of hydrous IDPs suggest that a cometary origin is uncertain and an asteroidal origin is at least as likely (e.g. Blake et al., 1988). A single grain of diopside was found in an anhydrous type. However, no Al or Ti enrichments were recorded in these grains. Thus no clear link between the C2063,1,154,1,0 grain and known IDP types is evident at present.

In contrast to the mesostasis-free C2063,1,154,1,0 grain, the C2061,1,113,5 particle does seem to have preserved traces of Na-rich silicate mesostasis. The mineral assemblage is consistent with being a fragment of a low-Ca pyroxene-bearing chondrule with Na-rich, silica-undersaturated mesostasis (Bridges et al., 1997). A mechanism to explain the presence of a Na-rich residual phase in the mesotasis is the extended metastable crystallisation of low-Ca pyroxene within a silicate chondrule melt. An alternative mechanism could be the influx of Na before the final cooling of the presumed surrounding chondrule (Bridges et al., 1997). Seven per cent of OC chondrules contain Na-rich mesostasis, with a higher proportion in carbonaceous chondrites (Grossman et al., 2000). Na-rich (kosmochloric) pyroxene has been identified in IDPs and in other *Stardust* tracks (Joswiak et al., 2009) associated with aluminosilicate glass or albitic feldspar. However as there is no Na enrichment in the C2061,1,113,5 pyroxene, this is not seen as a likely comparison.

In a TEM and oxygen isotope study of C2061,1,113,5, Nakamura-Messenger et al. (2011) showed that these phases were also present within other terminal particles from the same track, e.g. TP1-3. The nepheline was interpreted as having formed through devitrification of glass. They suggested that the glass and enstatite assemblage

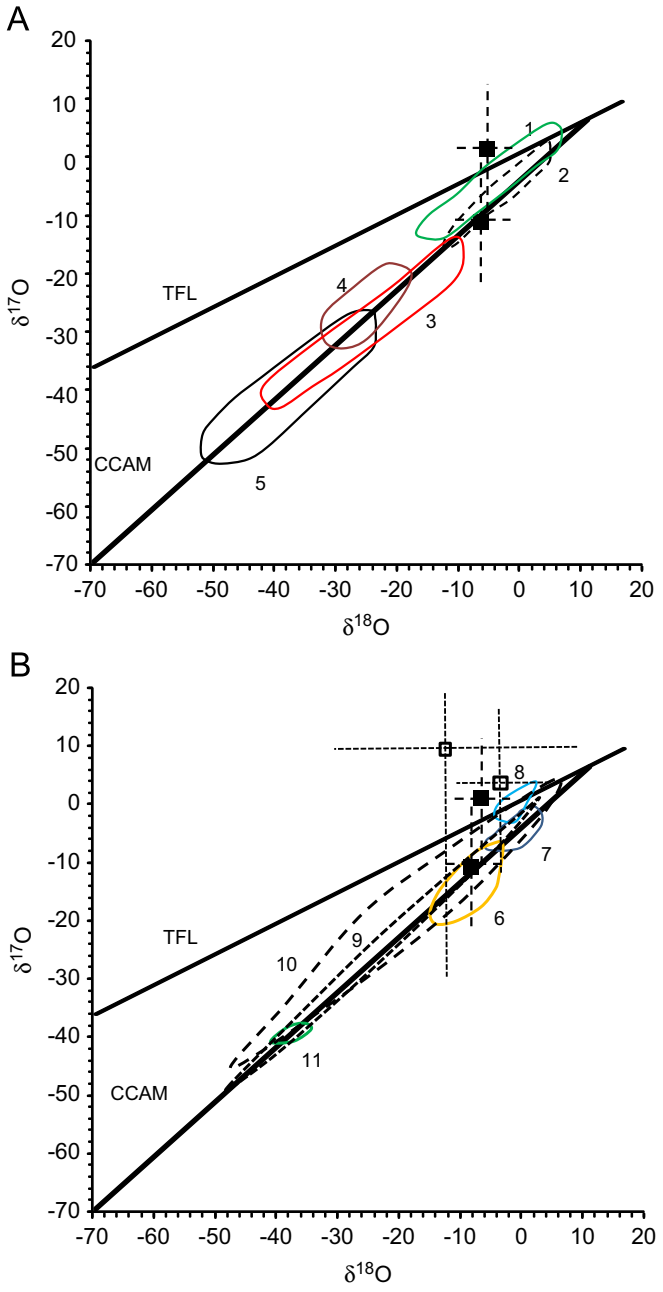

Fig. 8. (A,B) Three isotope plots of C2063,1,154,1,0, terminal grain 2 on slices C2063,1,154,1,15 and C2063,1,154,1,17 (black squares) with two sigma error bars shown for $\delta^{17}O$ and $\delta^{18}O$. Data in Table 2. Fields: 1. Al-rich bulk chondrules from ordinary chondrites. 2. Bulk chondrules from carbonaceous chondrites. 3. Diopside from Type C CAIs. 4. Al-diopside from CAIs in CV chondrites. 5. Minerals from Type A, B CAIs. 6. Al-rich chondrules (without relict CAI inclusions) from CR chondrites. 7. Al-diopside-rich bulk chondrules from CB chondrites. 8. Al-rich pyroxene from Al-rich chondrules in OCs. 9. ^{16}O-rich minerals within chondrules from Mokoia CV3 (Jones et al., 2004). 10. FeMg chondrule fragment ion probe analyses from Wild2 (Nakamura et al., 2008). 11. *Inti* CAI from Comet Wild 2 (Simon et al., 2008). Open squares Track 113 terminal grain analyses and 1 sigma errors (Nakamura-Messenger et al., 2011). CCAM: Carbonaceous Chondrites Anhydrous Minerals, TFL: Terrestrial Fractionation Line. Fields 1–8 are from Krot et al. (2001, 2006, 2008).

originated as nebula condensates. The identification of nebula condensates within primitive planetary materials is often uncertain, e.g. as within CAIs, most of which are now believed to have undergone melting (MacPherson, 2003). Stronger chemical evidence for nebula condensates has been identified in rare, ultrarefractory inclusions and refractory metal inclusions (Davis and Richter, 2003).

Table 2
Oxygen isotope analyses (‰).

Section	$\delta^{17}O$	2σ Error	$\delta^{18}O$	2σ Error	$\Delta^{17}O$
C2063,1,154,1,15	10.6	11.4	−7.5	5.0	−6.8
C2063,1,154,1,17	1.4	8.6	−6.5	3.2	4.8

$\Delta^{17}O = \delta^{17}IO - 0.52.\delta^{18}O$.

However, such phases do not clearly correspond to the C2061,1,113,5 grains. We suggest that a simpler explanation may be that this mineral assemblage is another fragment of a chondrule, similar to those with Na-rich, silica-undersaturated mesostases described in chondrites (Bridges et al., 1997). This would also be consistent with the oxygen isotope analyses of enstatite, nepheline-bearing terminal grains in C2061,1,113,5 (Nakamura-Messenger et al., 2011) which overlap the fields for chondrules (Fig. 8B).

Nakamura et al. (2008) described 4 crystalline particles, from various tracks, that are texturally, mineralogically, and compositionally similar to chondrules from carbonaceous chondrites. They consist of Mg-rich olivine, low-Ca pyroxene and traces of glassy mesostasis. In one case a microporphyritic texture typical of chondrules has been preserved. The *Toraijo* and *Gen Chan* chondrule fragments contain low-Ca pyroxene, e.g. $En_{80}Wo_3$ and En_{84-97} Wo_{11-2}, juxtaposed with aluminosilicate and Na-rich phases. Thus there is a possible similarity to the C2061,1,113,5 grain. These chondrule fragments show oxygen isotope compositions similar to chondrules in carbonaceous chondrites (Fig. 8B). Butterworth et al. (2010) also identified a chondrule fragment from Track 74 that showed traces of a microporphyritic texture with olivine, low-Ca pyroxene, glassy mesostasis and chrome spinel.

Some of the classic characteristics of chondrules: spherical outline, barred, radial or microporphyritic textures, or fine grained rims are not present in the samples from Tracks 154 and 113. However this is a near inevitable result of the fragmented nature of the preserved grains from the *Stardust* mission. Despite the challenge in accurately interpreting the samples, we suggest on the basis of our mineralogical and isotopic results that these samples are most readily explained as fragments of an Al-rich chondrule (C2063,1,154,1,0) and an FeMg chondrule (C2061,1,113,5). The beam sensitive nature of the Na-rich phase in the C2061,1,113,5 sample leaves open the possibility of a hydrous component. Partially hydrated Na-rich mesostases have been identified in chondrites (Grossman et al., 2000).

5.2. How were the chondrule fragments incorporated into Comet Wild2?

Nakamura et al. (2008) suggested that the presence of chondrule-like objects in Wild2 meant that chondrules have been transported out to the cold outer solar nebula and spread widely over the early Solar System. A similar suggestion was made by Simon et al. (2008), who proposed that the *Inti* CAI in Comet Wild2 had been transported outwards from the inner Solar System. Such envisaged transportation has the advantage that it can potentially explain the presence of high-temperature processed material within a region of space ~30 AU that, in traditional models of the Solar System, has temperatures that would not normally be expected to exceed 100 K.

However, chondrules in carbonaceous chondrites have mean diameters of 0.2–1.0 mm (Hutchison, 2004) which pose an unresolved challenge to such models. Hughes and Armitage (2010) presented the results from a series of models based on one-dimensional gas-disc evolution and particle transport models. Assuming plausible levels of turbulent diffusivity, such as those

invoked in transport models like that of Ciesla (2007) and used in *Stardust* interpretations such as those of Simon et al. (2008) and Chi et al. (2009), they demonstrated that particles in the size range 2– μm could reach the outer disc from the inner Solar System in a wide variety of models, as long as they were rapidly trapped within planetesimals. For particles of a few mm or larger, none of their models allowed outward transport to the comet-forming region 25–30 AU from anywhere in the inner Solar System. Even grains of a few hundreds of microns in size were predicted to be very rare because of their short residence times. Results from the *Stardust* Dust Flux Monitor suggest that the spacecraft encountered only a few grains >100 μm diameter, (Hörz et al., 2006) during its encounter with the comet's coma. It is in the nature of the *Stardust* record that we do not know for certain the original size distribution of grains within Comet Wild2. However, by analogy with carbonaceous chondrites, there is a reasonable probability that the chondrule fragments were hundreds of microns to 1 mm in diameter. Smaller chondrules 'microchondrules' are known in carbonaceous chondrites, but these are a volumetrically minor component compared to chondrules in the 0.2–1.0 mm size range (Krot et al., 1997).

One possible explanation is that chondrules were pulverised to dust within the inner Solar System (e.g. by asteroid impact), in which case some grains up to tens of microns might have been more readily transported to the comet-forming regions. An alternative scenario to explain our results is formation of high-T materials in situ at 25–30 AU. A 'Tidal Downsizing' model, based on simulations of Cha and Nayakshin (2011) and Vorobyov (2011), attempts to address such issues and considers the outer proto-planetary disc as gravitationally unstable and forming massive giant planet embryos (GEs) such as that of Jupiter (Nayakshin, 2010; Nayakshin et al., 2011). Heat is primarily released through contraction of the clumps with these hot (≤ 2000 K) and dense regions, situated in the background cold and low density disc, eventually being disrupted. The GE disruption is the result of increased tidal forces as GE migrate radially inward from their formation at >100 AU to tens of AU (e.g. Vorobyov and Basu, 2006). Disruption of GEs separates planets and small solids from the gas (Cha and Nayakshin, 2011).

The origin of chondrules is controversial (Scott and Krot, 2003), with a variety of competing models including nebular shocks (Cassen, 1996; Desch et al., 2010), lightning (Desch and Cuzzi, 2000), jets from near the proto-Sun (Shu et al., 2001) and impacts on partially molten planetesimals (e.g. Bridges et al., 1998; Hevey and Sanders, 2006). The maximum temperatures for chondrules are at least around the mineral liquidus temperatures of 1200–1500 K and perhaps higher (Desch et al., 2010).

Al–Mg analyses of an anorthite-rich, refractory particle—*Coki*, by Matzel et al. (2010) showed that this Comet Wild2 particle may have formed >1.7 Myr after the earliest Solar System objects. Al-rich chondrules in chondrites have also been dated with this ^{26}Al chronometer to show that they may have formed later than 1 Myr after CAIs (Huss et al., 2001; Kita et al., 2005). Assuming the chondrule fragments studied here are of similar age as *Coki* and Al-rich chondrules in chondrites then they might not have predated the GE planetary embryos. This would be consistent with models which envisage that chondrules are not progenitors of planetesimals and planets (including GEs) but rather formed a few Myr after the origin of the Solar System and the formation of planetary bodies. Within disrupted GEs, planetesimals would be expected through rapid growth of dust by collisional coagulation (Weidenschilling, 2000), triggering large grain sedimentation into the centres of GEs, and then gravitational collapse of grain-dominated regions into larger rocky objects (Nayakshin et al., 2011). Hevey and Sanders (2006) used the likely abundance of ^{26}Al shortly after the first few million years in the early Solar System to show that dust which rapidly accreted into $\sim$60 km, or larger, planetesimals would start melting.

The dispersion velocity of large objects within GEs can be as high as a fraction of a km/s (Nayakshin et al., 2011). Planetesimals as large as hundreds of kms across can be disrupted by impacts at such velocities or bow shocks (Boss, 2003) which may cause the sprays of melt droplets now seen preserved in chondrites. Impact models have the advantage of producing high volumes of chondrules (Scott and Krot, 2003). Shock or impact may also explain the presence of chondrule fragments within the *Stardust* collection of the Comet Wild2 coma. There is no evidence to suggest that the oxygen isotope systematics of the Wild2 samples differ significantly from those of meteoritic (asteroidal) materials. Therefore we speculate that the process of mass-independent fractionation of ^{16}O-depleted chondrule precursor solids from ^{16}O-rich solar gas that has been associated with the inner Solar System (McKeegan et al., 2011) may also have occurred within the outer Solar System. This scenario would require a diffuse radiation source, perhaps on the disc margins and/or in the interstellar medium prior to the onset of nebula collapse, to drive the mass-independent fractionation. If this scenario is accurate it would exclude the possibility of irradiation very close to the proto-Sun (e.g. Clayton, 2002). We suggest that the ^{16}O-rich compositions identified in our work are not definitive proof of an inner Solar System origin.

6. Conclusions

1. Terminal Grain 2 of C2063,1,154,1,0 from the *Stardust* collection of Comet Wild2 samples contains a fragment of an Al-diopside-rich chondrule. The mineral assemblage and Al_2O_3 contents are similar to Al-rich chondrules present in carbonaceous chondrites and the oxygen isotope composition is consistent with this. This is the first time such a particle has been identified within cometary material.
2. Terminal Grain 5 of C2061,1,113,5 consists of low-Ca pyroxene and up to 5–10% of a Na-rich, Si-poor glassy nepheline-like material similar to some mesostasis compositions from ferromagnesian chondrules in other *Stardust* samples and chondrites. We suggest an origin for the mesostasis composition through extended metastable crystallisation of low-Ca pyroxene in a chondrule melt rather than as nebula condensates, as suggested in a previous study of other C2061,1,113,5 terminal grains.
3. Our results add to the growing evidence for a large proportion of high-temperature, e.g. ≥ 1500 K, melted material within Comet Wild2. Rather than providing evidence for radial or X-wind transport mechanisms from the inner to outer Solar System, we speculate that such particles, which might originally have been in the size range of 0.2–1.0 mm, could be consistent with in-situ formation within the outer Solar System.

Acknowledgements

This work is funded by STFC Grants to JCB, SN at the University of Leicester and IAF at the Open University. Keiko Nakamura-Messenger, David Frank and Mike Zolensky of NASA-JSC are thanked for preparation of the microtome sections. HCG was an STFC Ph.D. student at UoL during this project. Graham Clark is thanked for assistance in the operation of the TEM. This paper benefited from 2 anonymous reviews.

References

Bischoff, A., Keil, K., 1983. Ca–Al-rich chondrules and inclusions in ordinary chondrites. Nature 303, 588–592.

Blake, D.F., Mardinly, A.J., Echer, C.J., Bunch, T.E., 1988. Analytical electron microscopy of a hydrated interplanetary dust particle. In: Proceedings of the 18th Lunar and Planetary Science Conference. Lunar and Planetary Institute, Houston, pp. 615–622.

Bockelée-Morvan, D., Gautier, D., Hersant, F., Hure, J.-M., Robert, F., 2002. Turbulent radial mixing in the solar nebula as the source of crystalline silicates in comets. Astron. Astrophys. 384, 1107–1118.

Boss, A.P., 2003. The solar nebula. In: Davies, A.M. (Ed.), Meteorites, Comets and Planets: Treatise on Geochemistry. Elsevier, pp. 63–82 (737 pp.).

Bridges, J.C., Alexander, C.M.O'D., Hutchison, R., Franchi, I.A., Pillinger, C.T., 1997. Na-, Cl-rich mesostases in Chainpur (LL3) and Parnallee (LL3) chondrules. Meteorit. Planet. Sci. 32, 555–565.

Bridges, J.C., Franchi, I.A., Hutchison, R., Sexton, A.S., Pillinger, C.T., 1998. Correlated mineralogy, chemical compositions, oxygen isotopic compositions and size of chondrules. Earth Planet. Sci. Lett. 155, 183–196.

Bridges, J.C., Franchi, I.A., Sexton, A.S., Pillinger, C.T., 1999. Mineralogical controls on the oxygen isotopic compositions of UOCs. Geochim. Cosmochim. Acta 63, 945–951.

Burchell, M.J., Fairey, S.A.J., Wozniakiewicz, P., Brownlee, D.E., Hörz, F., Kearsley, A.T., See, T.H., Westphal, A., Green, S.F., Trigo-Rodríguez, J.M., 2008. Characteristics of cometary dust tracks in Stardust aerogel and laboratory calibrations. Meteorit. Planet. Sci. 43, 23–40.

Butterworth, A.L., Gainsforth, Z., Bauville, A., Bonal, L., Brownlee, D.E., Fakra, S.C., Huss, G.R., Joswiak, D., Kunz, M., Marcus, M.A., Nagashima, K., Ogliore, R.C., Tamura, N., Telus, M.,Tyliszczak, T., Westphal, A.J., 2010. A Type IIa chondrule fragment from Comet 81P/Wild2 in Stardust Track C2052,2,74. In: Proceedings of the 40th Lunar and Planetary Science Conference, abstract no. 2446.

Cassen, P., 1996. Overview of models of the solar nebula: potential chondrule-forming events. In: Hewins, R., Jones, R., Scott, E. (Eds.), Chondrules and the Protoplanetary Disc. Cambridge University Press, pp. 21–28.

Cha, S.H., Nayakshin, S., 2011. A numerical simulation of a 'Super-Earth' core delivery from ~100 to ~8 AU. Mon. Not. R. Astron. Soc. 415, 3319.

Changela, H.G., 2011. Unpublished Ph.D. Thesis. University of Leicester, pp. 255.

Chi, M., Ishii, H.A., Simon, S.B., Bradley, J.P., Dai, Z., Joswiak, D., Browning, N.D., Matrajt, G., 2009. The origin of refractory minerals in comet 81P/Wild 2. Geochim. Cosmochim. Acta 73, 7150–7161.

Ciesla, F.J., 2007. Outward transport of high-temperature materials around the midplane of the solar nebula. Science 318, 613–615.

Clayton, R.N., 2002. Self-shielding in the solar nebula. Nature 415, 860–861.

Cliff, G., Lorimer, G.W., 1975. The quantitative analysis of thin specimens. J. Microsc. 103, 203–207.

Cox, K.G., Bell, J.D., Pankhurst, R.J., 1979. The Interpretation of Igneous Rocks. Allen & Unwin (450 pp.).

Davis, A.M., Richter, F.M., 2003. Condensation and evaporation of solar system materials. In: Davis, A.M. (Ed.), Treatise on Geochemistry, Vol. 1: Meteorites, Planets, and Comets, pp. 407–430.

Desch, S.J., Cuzzi, J.N., 2000. The generation of lightning in the solar nebula. Icarus 143, 87–105.

Desch, S.J., Morris, M.A., Connolly, H.C., Boss, A.P., 2010. A critical examination of the X-wind model for chondrule and calcium-rich, aluminum-rich inclusion formation and radionuclide production. Astrophys. J. 725, 692–711.

Grossman, L., Ebel, D.S., Simon, S.B., Davis, A.M., Richter, F.M., Parsad, N.M., 2000. Major element chemical and isotopic compositions of refractory inclusions in C3 chondrites: the separate roles of condensation and evaporation. Geochim. Cosmochim. Acta 64, 2879–2894.

Hevey, P.J., Sanders, I.S., 2006. A model for planetesimal meltdown by Al-26 and its implications for meteorite parent bodies. Meteorit. Planet. Sci. 41, 95–106.

Hörz, F., Bastien, R., Borg, J., Bradley, J.P., Bridges, J.C., Brownlee, D.E., Burchell, M.J., Chi, M., Cintala, M.J., Dai, Z.R., Djouadi, Z., Dominguez, G., Economou, T.E., Fairey, S.A.J., Floss, C., Franchi, I.A., Graham, G.A., Green, S.F., Heck, P., Hoppe, P., Huth, J., Ishii, H., Kearsley, A.T., Kissel, J., Leitner, J., Leroux, H., Marhas, K., Messenger, K., Schwandt, C.S., See, T.H., Snead, C., Stadermann, F.J., Stephan, T., Stroud, R., Teslich, N., Trigo-Rodríguez, J.M., Tuzzolino, A.J., Troadec, D., Tsou, P., Warren, J., Westphal, A., Wozniakiewicz, P., Wright, I., Zinner, E., 2006. Impact features on Stardust: implications for Comet 81P/Wild 2 dust. Science 314, 1716–1719.

Hughes, A.L.H., Armitage, P.J., 2010. Particle transport in evolving protoplanetary: implications for results from Stardust. Astrophys. J. 719, 1633–1653.

Huss, G.R., MacPherson, G.J., Wasserburg, G.J., Russell, S.S., Srinivasan, G., 2001. Aluminum-26 in calcium–aluminum-rich inclusions and chondrules from unequilibrated ordinary chondrites. Meteorit. Planet. Sci. 36, 975–997.

Hutchison, R., 2004. Meteorites: A Petrologic, Chemical and Isotopic Synthesis. Cambridge University Press (506 pp.).

Ishii, H.A., Bradley, J.P., Dai, Z.R., Chi, M.F., Kearsley, A.T., Burchell, M.J., Browning, N.D., Molster, F., 2008. Comparison of comet 81P/Wild 2 dust with interplanetary dust from comets. Science 319, 447–450.

Ito, M., Nagasawa, H., Yurimoto, H., 2004. Oxygen isotopic SIMS analysis in Allende CAI: details of the very early thermal history of the solar system. Geochim. Cosmochim. Acta 68, 2905–2923.

Jones, R.H., Leshin, L.A., Guan, Y., Sharp, Z.D., Durakiewicz, T., Schilk, A.J., 2004. Oxygen isotope heterogeneity in chondrules from the Mokoia CV3 carbonaceous chondrite. Geochim. Cosmochim. Acta 68, 3423.

Joswiak, D.J., Brownlee, D.E., Matrajt, G., Westphal, A.J., Snead, C.J., 2009. Kosmochloric Ca-rich pyroxenes and FeO-rich olivines (Kool grains) and associated phases in Stardust tracks and chondritic porous interplanetary dust particles: possible precursors to FeO-rich type II chondrules in ordinary chondrites. Meteorit. Planet. Sci. 44, 1561–1588.

Kita, N.T., Huss, G.R., Tachibana, S., Amelin, Y., Nyquist, L.E., Hutcheon, I.D., 2005. Constraints on the origin of chondrules and CAIs from short-lived and long-lived radionuclides. In: Krot, A.N., Scott, E.R.D., Reipurth, B. (Eds.), Chondrites and the Protoplanetary Disc, ASP Conference Series, vol. 341. Astronomical Society of the Pacific, San Francisco, pp. 558–587.

Kita, N.T., Nagahara, H., Tachibana, S., Tomomura, S., Spicuzza, M.J., Fournelle, J.H., Valley, J.W., 2010. High precision SIMS oxygen three isotope study of chondrules in LL3 chondrites: role of ambient gas during chondrule formation. Geochim. Cosmochim. Acta 74, 6610–6635.

Krot, A.N., Rubin, A.E., Keil, K., Wasson, J.T., 1997. Microchondrules in ordinary chondrites: implications for chondrule formation. Geochim. Cosmochim. Acta 61, 463–473.

Krot, A.N., McKeegan, K.D., Russell, S.S., Meobom, A., Weisberg, M.K., Zipfel, J., Krot, T.V., Fagan, T.J., Keil, 2001. Refractory calcium–aluminum-rich inclusions and aluminum-diopside-rich chondrules in the metal-rich chondrites Hammadah al Hamra 237 and Queen Alexandra Range 9411. Meteorit. Planet. Sci. 36, 1189–1216.

Krot, A.N., Yurimoto, H., McKeegan, K.D., Leshin, L., Chaussidon, M., Libourel, G., Yoshitake, M., Huss, G.R., Guan, Y., Zanda, B., 2006. Oxygen isotopic compositions of chondrules: implication for understanding oxygen isotope evolution of the solar nebula. Chem. Erde 66, 249–276.

Krot, A.N., Chaussidon, M., Yurimoto, H., Sakamoto, N., Nagashima, K., Hutcheon, I.D., MacPherson, G.J., 2008. Oxygen isotopic compositions of Allende Type C CAIs: evidence for isotopic exchange during nebular melting and asteroidal metamorphism. Geochim. Cosmochim. Acta 72, 2534–2555.

Li, Chunlai, Bridges, J.C., Hutchison, R., Ziyuan, Ouyang, 1998. Bo Xian (LL3.9): characterisation of separated chondrules. Meteorit. Planet. Sci. 35, 561–568.

Matzel, J.E.P., Ishii, H.A., Joswiak, D., Hutcheon, I.D., Bradley, J.P., Brownlee, D., Weber, P.K., Teslich, N., Matrajt, G., McKeegan, K.D., MacPherson, G.J., 2010. Constraints on the formation age of cometary material from the NASA stardust mission. Science 328, 483–486.

MacPherson, G.J., 2003. Calcium–aluminium rich inclusions in chondritic meteorites. In: Davis, A.M. (Ed.), Meteorites, Comets & Planets. Elsevier, pp. 737.

McKeegan, K.D., et al., 2006. Isotopic compositions of cometary matter returned by stardust. Science 314, 1724–1728.

McKeegan, K.D., Leshin, L.A., Russell, S.S., McPherson, G.J., 1998. Oxygen isotopic abundances in calcium–aluminum-rich inclusions from ordinary chondrites: implications for nebular heterogeneity. Science 280, 414–418.

McKeegan, K.D., Kallio, A.P.A., Heber, V.S., Jarzebinski, G., Mao, P.H., Coath, C.D., Kunihiro, T., Wiens, R.C., Nordholt, J.E., Moses Jr., R.W., Reisenfeld, D.B., Jurewicz, A.J.G., Burnett, D.S., et al., 2011. The oxygen isotopic composition of the sun inferred from captured solar wind. Science 332, 1528.

Nakamura, T., Noguchi, T., Tsuchiyama, A., Ushikubo, T., Kita, N.T., Valley, J.W., Zolensky, M.E., Kakazu, Y., Sakamoto, K., Mashio, E., Uesugi, K., Nakano, T., 2008. Chondrule like objects in short-period Comet 81P/Wild 2. Science 321, 1664–1667.

Nakamura-Messenger, K., Keller, L.P., Clemett, S.J., Messenger, S., Ito, M., 2011. nm-scale anatomy of entire Stardust tracks. Meteorit. Planet. Sci. 46, 1033–1051.

Nayakshin, S., 2010. Formation of terrestrial planet cores inside giant planet embryos. Mon. Not. R. Astron. Soc. 413, 1462–1478.

Nayakshin, S., Cha, S.H., Bridges, J.C., 2011. The tidal downsizing hypothesis for planet formation and the composition of Solar System comets. Mon. Not. R. Astron. Soc. 416, L50–L54.

Rietmeijer, F.J.M., 1998. Interplanetary dust particles in planetary materials. In: Papike, J.J. (Ed.), Reviews in Mineralogy, vol. 36. Mineralogical Society of America, pp. 3-1–3-398.

Russell, S.S., MacPherson, G.J., Leshin, L.A., McKeegan, K.D., 2000. ^{16}O enrichments in aluminium-rich chondrules from ordinary chondrites. Earth. Planet. Sci. Lett. 184, 57–74.

Scott, E.R.D., Krot, A.N., 2003. Chondrites and their components. In: Davis, A.M. (Ed.), Meteorites, Comets and Planets: Treatise on Geochemistry, vol. 1. Elsevier, pp. 143–246 (737 pp.).

Shu, F.H., Shang, H., Glassgold, A.E., Lee, T., 1997. X-rays and fluctuating X-winds from protostars. Science 277, 1475–1479.

Shu, F.H., Shang, H., Gounelle, M., Glassgold, A.E., 2001. The origin of chondrules and refractory inclusions in chondritic meteorites. Astrophys. J. 548, 1029–1050.

Simon, S.B., Joswiak, D.J., Ishii, H.A., Bradley, J.P., Chi, M.F., Grossman, L., Aléon, L., Brownlee, D.E., Fallon, S., Hutcheon, I.D., Matrajt, G., McKeegan, K.D., 2008. A refractory inclusion returned by Stardust from Comet 81P/Wild 2. Meteorit. Planet. Sci. 43, 1861–1877.

Tomeoka, K., Buseck, P.R., 1985. Hydrated interplanetary dust particle linked with carbonaceous chondrites? Nature 314, 338–340.

Vorobyov, E.I., 2011. Destruction of massive fragments in protostellar disks and crystalline silicate production. Astrophys. J. Lett. 728, L45.

Vorobyov, E.I., Basu, S., 2006. The burst mode of protostellar accretion. Astrophys. J. 650, 956.

Weidenschilling, S.J., 2000. Formation of planetesimals and accretion of the terrestrial planets. Space Sci. Rev. 92, 295–310.
Westphal, A.J., Fakra, S.C., Gainsforth, Z., Marcus, M.A., Ogliore, R.C., Butterworth, A.L., 2009. Mixing fraction of inner solar system material in Comet 81P/Wild2. Astrophys. J. 694, 18–28.
Zolensky, M.E., Barrett, R.A., 1994. Compositional variations of olivines and pyroxenes in chondritic interplanetary dust particles. Meteoritics 29, 616–620.
Zolensky, M.E., Zega, T.J., Yano, H., Wirick, S., Westphal, A.J., Weisberg, M.K., Weber, I., Warren, J.L., Velbel, M.A., Tsuchiyama, A., Tsou, P., Toppani, A., Tomioka, N., Tomeoka, K., Teslich, N., Taheri, M., Susini, J., Stroud, R., Stephan, T., Stadermann, F.J., Snead, C.J., Simon, S.B., Simionovici, A., Rietmeijer, F.J.M., Rao, I., Perronnet, M.C., Papanastassiou, D.A., Okudaira, K., Ohsumi, K., Ohnishi, I., Nakamura-Messenger, K., Nakamura, T., Mostefaoui, S., Mikouchi, T., Meibom, A., Matrajt, G., Marcus, M.A., Leroux, H., Lemelle, L., Le, L., Lanzirotti, A., Langenhorst, F., Krot, A.N., Keller, L.P., Kearsley, A.T., Joswiak, D., Jacob, D., Ishii, H., Harvey, R., Hagiya, K., Grossman, L., Grossman, J.N., Graham, G.A., Gounelle, M., Gillet, Ph, Genge, M.J., Flynn, G., Ferroir, T., Fallon, S., Ebel, D.S., Dai, Z.R., Cordier, P., Clark, B., Chi, M., Butterworth, A.L., Brownlee, D.E., Bridges, J.C., Brennan, S., Brearley, A., Bradley, J.P., Bleuet, P., Bland, P.A., Bastien, R., 2006. Mineralogy and petrology of Comet 81P/Wild 2 nucleus samples. Science 314, 1735–1739.